Journal of Bio- and Tribo-Corrosion (2018) 4:64
https://doi.org/10.1007/s40735-018-0179-3

4-(2-(2-(2-(2-(Pyridine-4-yl)ethylthio)ethoxy)ethylthio)ethyl)pyridine as New Corrosion Inhibitor for Mild Steel in 1.0 M HCl Solution: Experimental and Theoretical Studies

A. Khadiri[1] · A. Ousslim[1] · K. Bekkouche[1] · A. Aouniti[2] · I. Warad[3] · A. Elidrissi[2] · B. Hammouti[2] · F. Bentiss[4] · M. Bouachrine[5] · A. Zarrouk[2]

Received: 9 June 2018 / Revised: 14 August 2018 / Accepted: 27 August 2018 / Published online: 6 September 2018

Abstract
The inhibition effect of 4-(2-(2-(2-(2-(pyridine-4-yl)ethylthio)ethoxy)ethylthio)ethyl)pyridine (P4E4P) on mild steel corrosion in 1.0 M HCl solution was investigated by quantum chemical calculations, electrochemical techniques, and weight loss measurements. The experimental results reveal that this compound has a good inhibiting effect and the inhibition efficiency, increased with the inhibitor concentration to reach 97% at 1 mM. The effect of temperature on the corrosion behavior of mild steel has been examined in the temperature range of 308–353 K. The inhibition efficiency increases with increasing inhibitor concentration, but decreases with increasing temperature. The adsorption of the inhibitor on mild steel surface obeyed the Langmuir adsorption isotherm. The kinetic and thermodynamic parameters for mild steel corrosion and inhibition adsorption, respectively, were determined and discussed. Potentiodynamic polarization suggested that it is a mixed type of inhibitor. Data obtained from EIS measurements were analyzed to model the corrosion inhibition process through the appropriate equivalent circuit model. Quantum chemical calculations were employed to study the electronic properties of P4E4P to ascertain the correlation between the inhibitory effect and the molecular structure. Both the experimental and theoretical results are in good agreement with each other in this regard and confirm that P4E4P is an effective inhibitor.

Keywords Pyridine derivative · Mild steel · Corrosion inhibition · Adsorption · Theoretical study

1 Introduction

The use of organic compounds as corrosion inhibitors plays a significant role in reducing corrosion of industrial metals and alloys in an acidic environment encountered during processing of metals and alloys [1]. By considering the practical applications of acidic solutions at various industrial processes such as acid pickling of steel, scale removal in metallurgy, acid cleaning of boilers and oil-well acidizing, hydrochloric acids are most widely used for all these purposes. However, the strong corrosion of hydrochloric acid needs to be controlled by an appropriate corrosion inhibitor [2–5]. The organic compounds containing a heteroatom such as phosphorus, sulfur, nitrogen, or those containing multiple bonds, which are considered as adsorption centers, are effective inhibitors for the corrosion of metals [6–13]. The efficiency of these compounds as corrosion inhibitors can be attributed to a number of mobile electron pair present, the π orbital character of free electrons and the electron density around heteroatoms [14–16]. Many organic compounds containing pyridine and heteroatom have been used for the corrosion inhibition of steel in acidic media [17–22].

Theoretical chemistry, including quantum chemical calculation, has been proved to be a very powerful tool for studying the mechanism of corrosion inhibition [23]. This theoretical approach has been widely used to investigate

✉ A. Zarrouk
azarrouk@gmail.com

1 LCSMA - Faculté des Sciences, Université Mohammed Premier, PO Box 717, 60000 Oujda, Morocco

2 LC2AME, Faculty of Science, Mohammed First University, PO Box 717, 60000 Oujda, Morocco

3 Department of Chemistry, AN-Najah National University, PO Box 7, Nablus, Palestine

4 Laboratoire de Catalyse et de Corrosion des Matériaux (LCCM), Faculté des Sciences, Université Chouaib Doukkali, PO Box 20, 24000 El Jadida, Morocco

5 ESTM, Université Moualy Ismail, Meknes, Morocco

a correlation between molecular structure and inhibition efficiency of an organic compound [24, 25]. Therefore, it is worthwhile to compute the structural parameters including the highest occupied molecular orbital energy (E_{HOMO}), the lowest unoccupied molecular orbital (E_{LUMO}), dipole moment (μ), etc.

In this work, corrosion inhibition of 4-(2-(2-(2-(2-(pyridine-4-yl)ethylthio)ethoxy)ethylthio)ethyl)pyridine (P4E4P) on mild steel in hydrochloric acid solution has been studied. Weight loss measurements, electrochemical methods, including potentiodynamic polarization and electrochemical impedance spectroscopy (EIS) have been employed to investigate the effect of concentration and temperature on the inhibiting behavior of this compound. Also, the quantum chemical method has been used for identification of adsorption type and modeling corrosion inhibition by means of quantum chemical indices.

2 Experimental Details

2.1 Materials

The material used in this study is mild steel with a chemical composition in (wt%) of 0.21% C, 0.38% Si, 0.05% Mn, 0.05% S, 0.09% P, 0.01% Al, and the remainder iron (Fe). The steel samples were pre-treated prior to the experiments by grinding with emery paper SiC (120, 600, 1200, and 2000); rinsed with distilled water.

2.2 Solutions

The aggressive solutions of 1.0 M HCl were prepared by dilution of analytical grade 37% HCl with distilled water. The concentration range of 4-(2-(2-(2-(2-(pyridine-4-yl)ethylthio)ethoxy)ethylthio)ethyl)pyridine (P4E4P) used was 1×10^{-6} M to 1×10^{-3} M.

2.3 Synthesis

A mixture of 4-vinylpyridine (21.02 g, 0.2 mol) and 2, 2-azo-bis-isobutyronitrile (AIBN) (0.082 g, 5×10^{-4} mol) in 100 mL of acetonitrile was added drop by drop during 30 min to 2-mercaptoethylether dissolved in 50 mL of acetonitrile. After, the mixture was stirred during 3 h in the presence of pure nitrogen (N_2) at 70 °C in atmospheric pressure. The solvent and the excess of 2-mercaptoethylether were removed and the product was purified by chromatographic on a silica column (eluant, CH_2Cl_2), to give product P4E4P as a viscous dark red liquid, Yield 90%. A schematic representation of the synthesis is shown in Scheme 1. This inhibitor was synthesized according to A. Ousslim in our laboratory and characterized by IR spectroscopy (Fig. 1), ^{1}H-NMR (Fig. 2) and ^{13}C-NMR (Fig. 3).

^{1}H-NMR ($CDCl_3$, δ (ppm)): 2.77 (m, 6H); 3.68 (t, 2H); 7.14 (d, 2H); 8.46 (d, 2H), ^{13}C-NMR ($CDCl_3$, δ (ppm)): 31.9; 32.2; 38.2; 72.2; 120.75; 144.63; 150.26; IR (KBr, ν (cm^{-1})): 2999 (FF); 2870 (FF); 1600 (F); 1400 (F); 1200–1111 (FF); 904 (m); 600 (f).

2.4 Corrosion Tests

2.4.1 Gravimetric Measurements

The gravimetric measurements were carried out at a definite time interval of 6 h at room temperature using an analytical balance (precision ± 0.1 mg). The mild steel specimens used rectangular form (length = 1.3 cm, width = 1.3 cm, thickness = 0.13 cm). Gravimetric experiments were carried out in a double glass cell equipped with a thermostated cooling condenser containing 50 mL of non-de-aerated test solution.

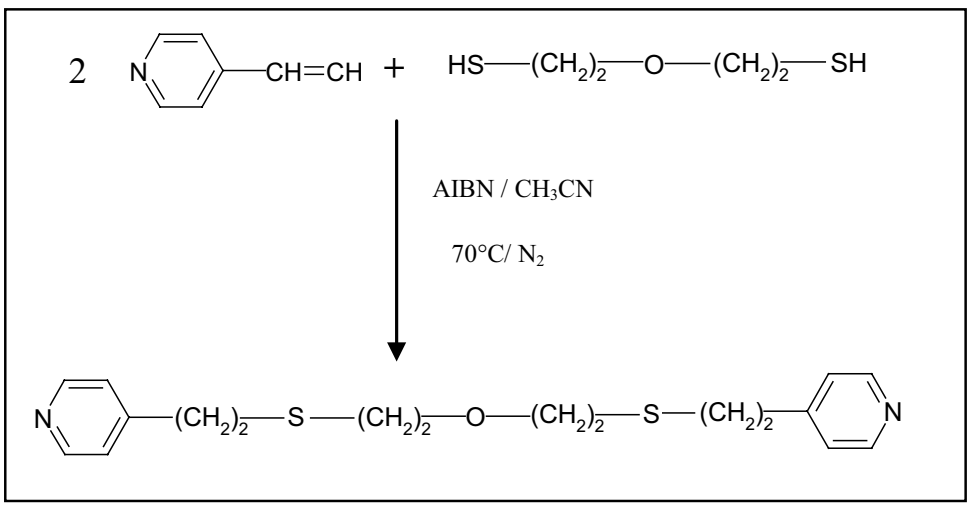

Scheme 1 Structure and synthetic route of 4-(2-(2-(2-(2-(pyridine-4-yl)ethylthio)ethoxy)ethylthio)ethyl)pyridine (P4E4P)

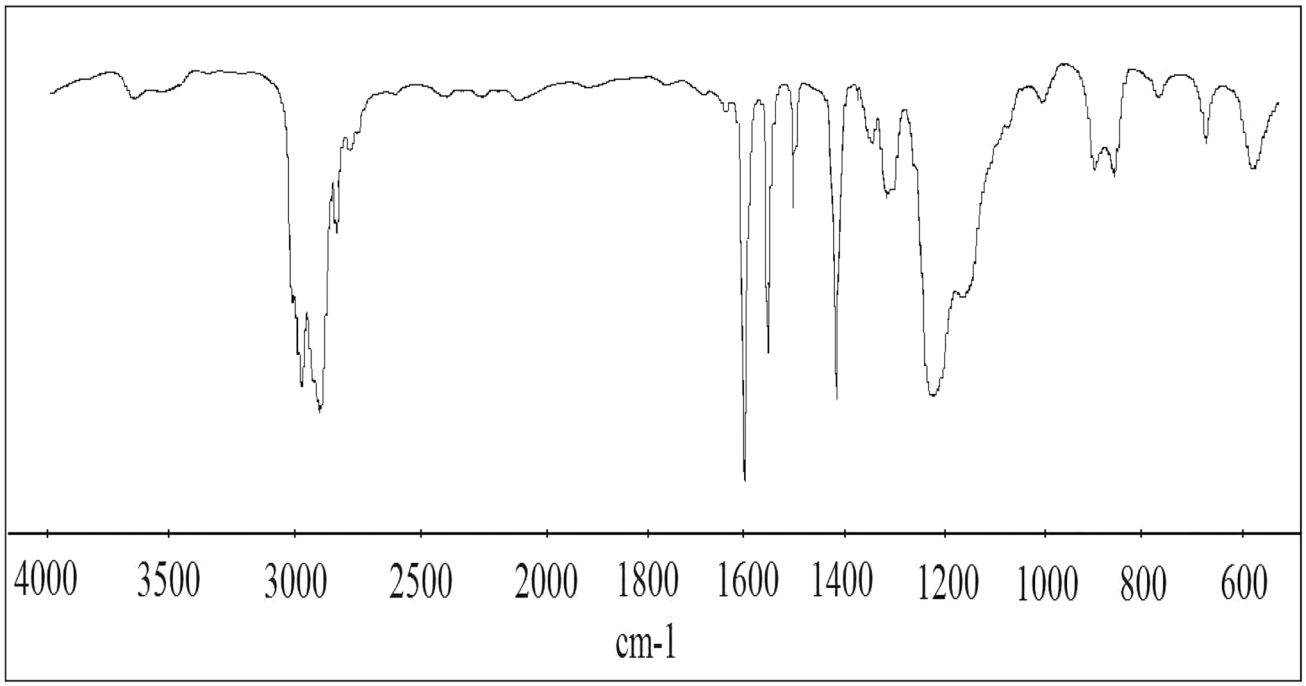

Fig. 1 IR spectrum of 4-(2-(2-(2-(2-(pyridine-4-yl)ethylthio)ethoxy)ethylthio)ethyl)pyridine (P4E4P)

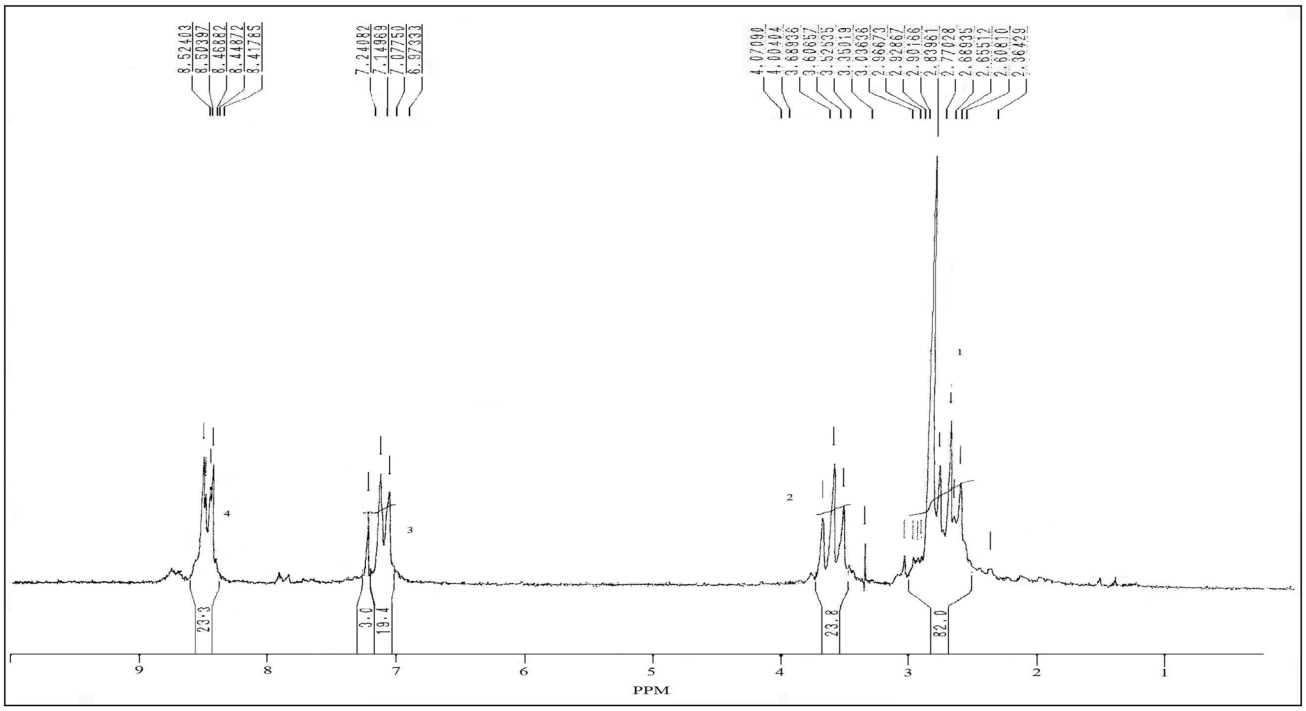

Fig. 2 ^{1}H NMR spectrum of 4-(2-(2-(2-(2-(pyridine-4-yl)ethylthio)ethoxy)ethylthio)ethyl)pyridine (P4E4P)

After the immersion period, the steel specimens were withdrawn, carefully rinsed with bidistilled water, ultrasonic cleaning in acetone, dried at room temperature and then weighted. The corrosion rate (ν) in mg cm^{-2} h^{-1} was calculated from the following equation [26]:

$$\nu = \frac{W}{St} \quad (1)$$

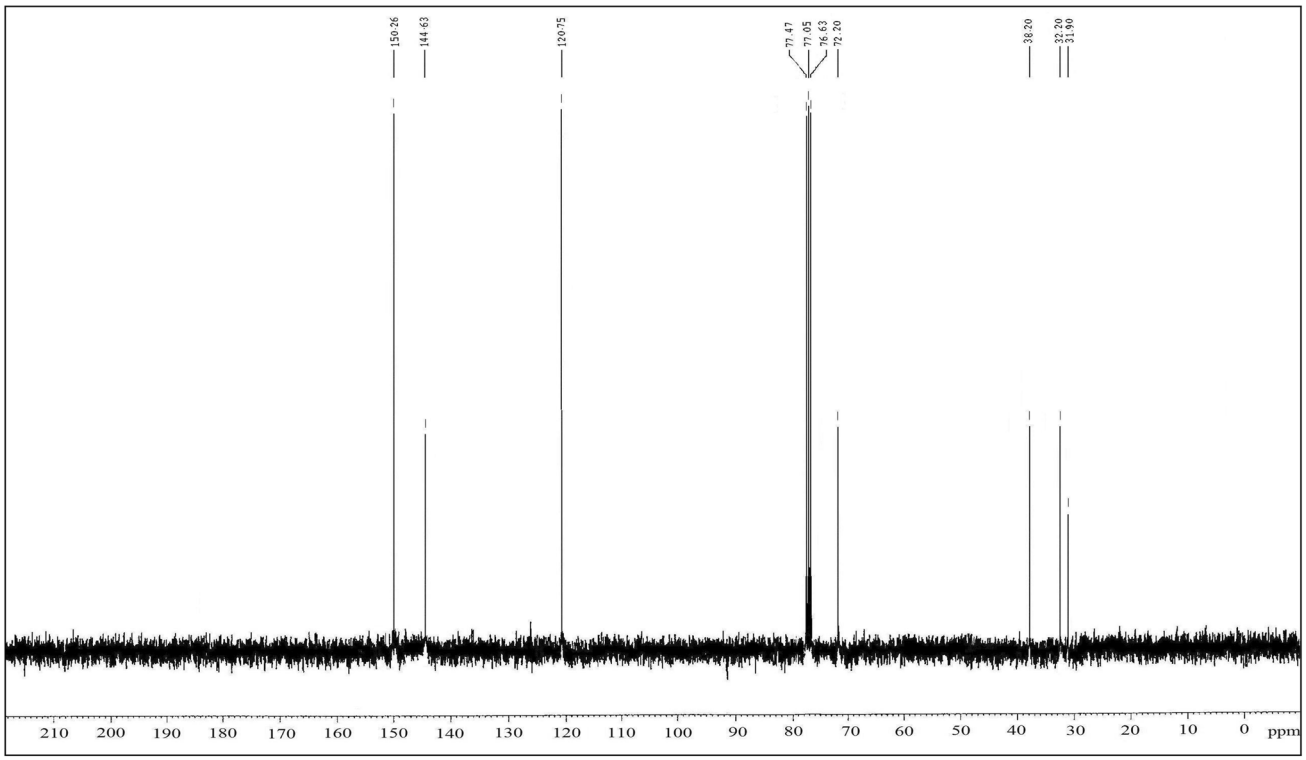

Fig. 3 ^{13}C NMR spectrum of 4-(2-(2-(2-(2-(pyridine-4-yl)ethylthio)ethoxy)ethylthio)ethyl)pyridine (P4E4P)

$$\eta_{WL}(\%) = \frac{\nu_0 - \nu}{\nu_0} \times 100 \quad (2)$$

where W is the three-experiment average weight loss of the mild steel; S is the total surface area of the specimen; t is the immersion time, and ν_0 and ν are the values of the corrosion rate without and with the addition of the inhibitor, respectively.

The fractional surface coverage θ can be easily determined from weight loss measurements by the ratio $\eta_{WL}(\%)/100$ if one assumes that the values of $\eta_{WL}(\%)$ do not differ substantially from θ.

2.4.2 Electrochemical Measurements

The electrochemical measurements were carried out using Volta lab (Tacussel-Radiometer PGZ 100) potentiostat and controlled by Tacussel corrosion analysis software model (Voltamaster 4) at under static condition. The corrosion cell used had three electrodes. The reference electrode was a saturated calomel electrode (SCE). A platinum electrode was used as an auxiliary electrode of the surface area of 1 cm^2. The working electrode was mild steel. All potentials given in this study were referred to this reference electrode. The working electrode was immersed in the test solution for 60 min to a establish steady state open circuit potential (E_{ocp}). After measuring the E_{ocp}, the electrochemical measurements were performed. All electrochemical tests have been performed in aerated solutions at 308 K. The EIS experiments were conducted in the frequency range with a high limit of 100 kHz and different low limit 0.01 Hz at open circuit potential, with 10 points per decade, at the rest potential, after 60 min of acid immersion, by applying 10 mV ac voltage peak-to-peak. Nyquist plots were made from these experiments. The impedance data were analyzed and fitted with the simulation ZView 2.80, equivalent circuit software.

After the AC impedance test, the potentiodynamic polarization measurements of mild steel substrate in inhibited and uninhibited solution were scanned from cathodic to the anodic direction between −800 mV and −200 mV, with a scan rate of 1 mV s^{-1}. The potentiodynamic data were analyzed using the polarization VoltaMaster 4 software. The linear Tafel segments of anodic and cathodic curves were extrapolated to corrosion potential to obtain corrosion current densities (i_{corr}). From the polarization curves obtained, the corrosion current (i_{corr}) was calculated by curve fitting using the equation:

$$i = i_{corr}\left[\exp\left(\frac{2.3\Delta E}{\beta_a}\right) - \exp\left(\frac{2.3\Delta E}{\beta_c}\right)\right] \quad (3)$$

β_a and β_c are the anodic and cathodic Tafel slopes and ΔE is $E - E_{corr}$.

The inhibition efficiency was evaluated from the measured i_{corr} values using the following relationship:

$$h_{Tafel}(\%) = \frac{i_{corr} - i_{corr(i)}}{i_{corr}} \times 100 \quad (4)$$

where i_{corr} and $i_{corr(i)}$ are the corrosion current densities for the steel electrode in the uninhibited and inhibited solutions, respectively.

2.5 Computational Procedures

Density functional theory (DFT) has been recently used [27–30], to describe the interaction between the inhibitor molecule and the surface as well as the properties of these inhibitors concerning their reactivity. The molecular band gap was computed as the first vertical electronic excitation energy from the ground state using the time-dependent density functional theory (TD-DFT) approach as implemented in Gaussian 03 [31]. For these seek, some molecular descriptors, such as HOMO and LUMO energy values, frontier orbital energy gap, molecular dipole moment, electronegativity (χ), global hardness (η), softness (σ), were calculated using the DFT method and have been used to understand the properties and activity of the newly prepared compounds and to help in the explanation of the experimental data obtained for the corrosion process.

According to Koopman's theorem [32], the ionization potential (IE) and electron affinity (EA) of the inhibitors are calculated using the following equations:

$$IE = -E_{HOMO} \quad (5)$$

$$EA = -E_{LUMO} \quad (6)$$

Thus, the values of the electronegativity (χ) and the chemical hardness (η) according to Pearson, operational and approximate definitions can be evaluated using the following relations [33]:

$$\chi = \frac{IE + EA}{2} \quad (7)$$

$$\eta = \frac{IE - EA}{2} \quad (8)$$

Global chemical softness (σ), which describes the capacity of an atom or group of atoms to receive electrons [28], was estimated by using the equation:

$$\sigma = \frac{1}{\eta} = -\frac{2}{E_{HOMO} - E_{LUMO}} \quad (9)$$

3 Results and Discussions

3.1 Potentiodynamic Polarization

Tafel plots generated from potentiodynamic polarization curves for mild steel in 1.0 M HCl with various concentrations (from 10^{-6} to 10^{-3} M) of P4E4P as an inhibitor at 308 K are shown in Fig. 4. A prominent decrease in the corrosion rate occurred because of the addition of P4E4P in HCl medium. The corrosion parameters, including corrosion potential (E_{corr}), corrosion current density (i_{corr}), Tafel slope values (β_a and β_c) and inhibition efficiency (η_{Tafel}), obtained from the curves in Fig. 1 are summarized in Table 1.

The results also indicate that the inhibition efficiencies increased with the concentration of inhibitor. Such behavior can be interpreted on the basis that the inhibitor acts by adsorbing onto the metal surface. In acidic solutions, the anodic reaction of corrosion is the passage of metal ions from the metal surface into the solution, and the cathodic reaction is the discharge of hydrogen ions to produce hydrogen gas or to reduce oxygen. The inhibitor may affect either the anodic or the cathodic reaction, or both [34]. Because the anodic Tafel slope (β_a) and cathodic Tafel slope (β_c) of P4E4P were found to change with inhibitor concentration, the inhibitor had thus affected both of these reactions [35]. P4E4P can thus be classified as an anodic- or cathodic-type inhibitor when the change in the E_{corr} value is greater than 85 mV [36]. Because the largest displacement exhibited by P4E4P was 44 mV at 308 K (Table 1), it may be concluded that this molecule should be considered a mixed-type inhibitor, meaning that the addition of P4E4P to a 1.0 M HCl solution both reduces the anodic dissolution of mild steel and retards the cathodic hydrogen evolution reaction. The

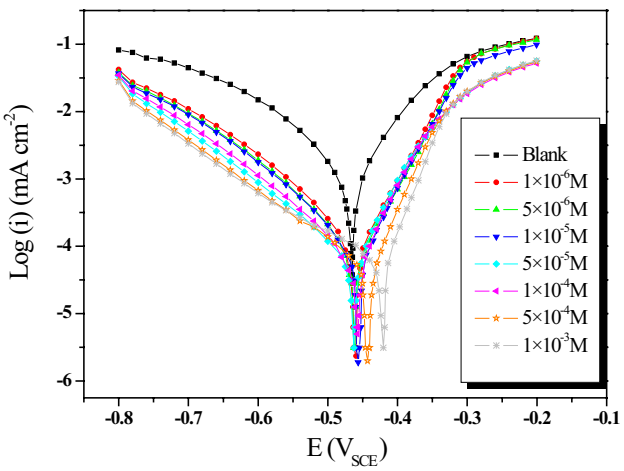

Fig. 4 Potentiodynamic polarization curves for mild steel in 1.0 M HCl without and with different concentrations of P4E4P

Table 1 Polarization parameters and the corresponding inhibition efficiency of mild steel corrosion in 1.0 M HCl containing different concentrations of P4E4P at 308 K

C_{inh} (M)	E_{corr} (mV/SCE)	$-\beta_a$ (mV dec^{-1})	$-\beta_c$ (mV dec^{-1})	i_{corr} (μA cm^{-2})	η_{Tafel} (%)
Blank	−467	71.1	101.0	966	–
1×10^{-6}	−464	63.6	103.9	126	86.9
5×10^{-6}	−464	69.0	100.6	95	90.2
1×10^{-5}	−459	56.0	100.5	79	91.8
5×10^{-5}	−463	48.0	104.5	51	94.8
1×10^{-4}	−460	50.4	101.0	50	94.8
5×10^{-4}	−444	43.7	115.8	43	95.5
1×10^{-3}	−423	37.9	147.2	36	96.3

presence of increasing amounts of P4E4P led to a decrease in both the cathodic and anodic current densities. Adsorption is the mechanism that is generally accepted to explain the inhibitory action of organic corrosion inhibitors. The adsorption of inhibitors can affect the corrosion rate in two ways: (i) by decreasing the available reaction area, i.e., the so-called geometric blocking effect, and (ii) by modifying the activation energy of the cathodic and/or anodic reactions occurring in the inhibitor-free metal in the course of the inhibited corrosion process. It is a difficult task to determine which aspects of the inhibiting effect are connected to the geometric blocking action and which are connected to the energy effect. Theoretically, no shifts in E_{corr} should be observed after the addition of the corrosion inhibitor if the geometric blocking effect is stronger than the energy effect [34]. Compared with the earlier studied pyridine derivative corrosion inhibitors in Table 2, P4E4P exhibited better corrosion inhibition behavior. This phenomenon is related to the molecular size and the number of heteroatoms in the structure.

3.2 Electrochemical Impedance Spectroscopy Measurements (EIS)

In order to confirm the results extracted from potentiodynamic polarization and to obtain more information about corrosion mechanisms, EIS measurements were carried out at the open circuit potential E_{OCP}. The Nyquist plots obtained for mild steel in 1.0 M HCl in the absence and presence of various concentrations of the inhibitor are shown in Fig. 5a. It can be seen that the impedance diagrams show for all concentration a depressed capacitive loop in the high-frequency (HF) range and inductive loop (except for 5×10^{-5} M and 1×10^{-4} M) in the lower frequency (LF) range. The (HF) capacitive loops can be attributed to the charge transfer process predominantly influences the corrosion inhibition of mild steel. The diameter of capacitive loops significantly increases, suggesting that the inhibition rate increases with the addition of P4E4P. The presence of the (LF) inductive loops may be attributed to the relaxation process obtained by adsorption species like Cl^-_{ads}, H^+_{ads} on the electrode surface [41–46]. It may also be attributed to the adsorption of the inhibitor on the electrode surface [43, 46, 47] or to the redissolution of the passivity surface at low frequencies [48]. In other words, the inductive behavior at low frequencies is probably due to the adsorption of the products of the corrosion on the electrode surface (for example $FeOH_{ads}$ and FeH_{ads}) [49].

The Bode-phase diagrams (Fig. 5b) consist of a single wave crest and a portion of curve under the zero phase degree, the increase of absolute impedance at low frequencies in Bode plots confirms the higher protection with increasing the concentration of inhibitor, which is related to the adsorption of P4E4P molecules on the mild steel surface in 1.0 M HCl [50, 51]. However, it is also clear that the shapes of the impedance plots for the inhibited electrodes are not essentially different from those of the uninhibited electrode. According to the appearance of

Table 2 Comparison of the inhibition efficiency of P4E4P with the literature data as corrosion inhibitors for mild steel in HCl solution

Inhibitor	C_{inh} (M)	η (%)	Ref.
4-(2-(2-(2-(2-(pyridine-4-yl)ethylthio)ethoxy)ethylthio)ethyl) pyridine (P4E4P)	10^{-3}	96.3	This paper
4-(dodecylthiaethyl)pyridine (DTEP)	10^{-3}	90.1	[37]
4-pyridylethylthia-acetic acid (PETAA)	10^{-3}	83.6	[37]
2-(3-methyl-1H-pyrazol-5-yl)pyridine (P3)	10^{-3}	91.0	[38]
(5-methyl-1-pyridin2-yl-1H-pyrazol-3-yl)methanol (P1)	10^{-3}	92.0	[39]
3-pyridinecarboxaldehyde-4-phenyl thiosemicarbazide (3-PCPTC)	10^{-3}	90.0	[40]
4-pyridinecarboxaldehyde-4-phenylthiosemicarbazide (4-PCPTC)	10^{-3}	89.0	[40]

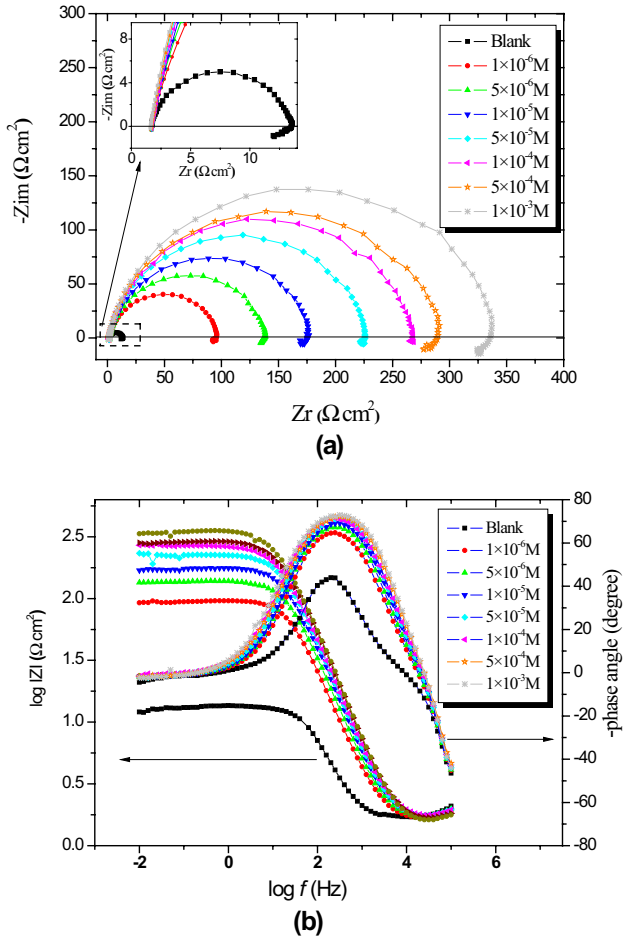

Fig. 5 **a** EIS Nyquist and **b** Bode diagrams for carbon steel/1.0 M HCl + different concentrations of inhibitor at 308 K

phase angle plots, increasing the concentration of inhibitor in 1.0 M HCl solutions results in more negative values of phase angle indicating superior inhibitive behavior due to P4E4P molecules adsorbed on a metal surface at higher concentrations.

Electrical equivalent circuits are generally used to model the electrochemical behavior and to calculate the impedance parameters [52]. The simple equivalent circuit for data fitting and the measured and fitted curves are shown in Fig. 6. According to the proposed equivalent circuit, the fitted curves are compared well with those from the experiment. In these circuits, R_s represents the solution resistance; R_{ct} is the charge transfer resistance; R_a is the resistance of the adsorbed inhibitor; L is the inductance; R_L is the inductance resistance; CPE_d is the constant phase element of the high-frequency semicircle that can be attributed to the charge transfer process; CPE_a is the constant phase element of the inhibitor film due to the adsorbed molecules of inhibitor.

The constant phase element CPE is introduced in the circuit instead of a pure double-layer capacitor to give a more accurate fit [24, 53]. The impedance of the CPE is expressed by the following expression:

$$Z_{CPE} = \frac{1}{A(iw)^n} \tag{10}$$

where A (Ω^{-1} s^n cm^{-2}) is the magnitude of the CPE; w (rad s^{-1}) is the sine wave modulation angular frequency; $i^2 = -1$ is the imaginary number and n is an empirical exponent which measures the deviation from the ideal capacitive behavior [54, 55]. Depending on the values of n, CPE can represent resistance ($n = 0$), capacitance ($n = 1$), inductance ($n = -1$), and Warburg impedance ($n = 0.5$) [43, 56–59]. The values of double-layer capacitance C_{dl} derived from the CPE_d and the values of adsorption capacitance C_a derived from the CPE_a can be calculated using Eqs. (11) and (12), respectively [19].

$$C_{dl} = \sqrt[n_d]{A_d (R_{ct})^{1-n_d}} \tag{11}$$

$$C_a = \sqrt[n_a]{A_a (R_a)^{1-n_a}} \tag{12}$$

The relaxation time constant (τ_d) of charge-transfer process and the time constant (τ_a) of the adsorption process can be calculated by Eqs. (13) and (14), respectively [19].

$$\tau_d = C_{dl} R_{ct} \tag{13}$$

$$\tau_a = C_a R_a \tag{14}$$

The related inhibition efficiency, η_Z (%), is calculated from $R_p = (R_{ct} + R_L + R_a)$ using the following Eq. (15):

$$\eta_Z(\%) = \left(\frac{R_P - R_P^\circ}{R_P^\circ} \right) \times 100 \tag{15}$$

where R_p° and R_P are the ac polarization resistance of mild steel electrode in the uninhibited and inhibited solutions, respectively.

The impedance parameters and the inhibition efficiency are calculated and listed in Table 3. Inspection of data in this table clearly shows that in the whole concentration range, the charge transfer resistance R_{ct} increases with P4E4P concentration; hence the better inhibition power is achieved. This effect is connected with simultaneous decrease of double-layer capacitance (C_{dl}) often observed when adsorption of organic molecules on the electrode surface takes place [60]. In addition, the value of the proportional factor A_d of CPE_d varies in a regular manner with inhibitor concentration. The increase of n_d values with concentration can be attributed to a certain decrease in the initial surface in homogeneity resulting from the adsorption of P4E4P molecules on the most active adsorption centers at the mild steel surface [61]. Indeed the values of n_d are close to unity which shows

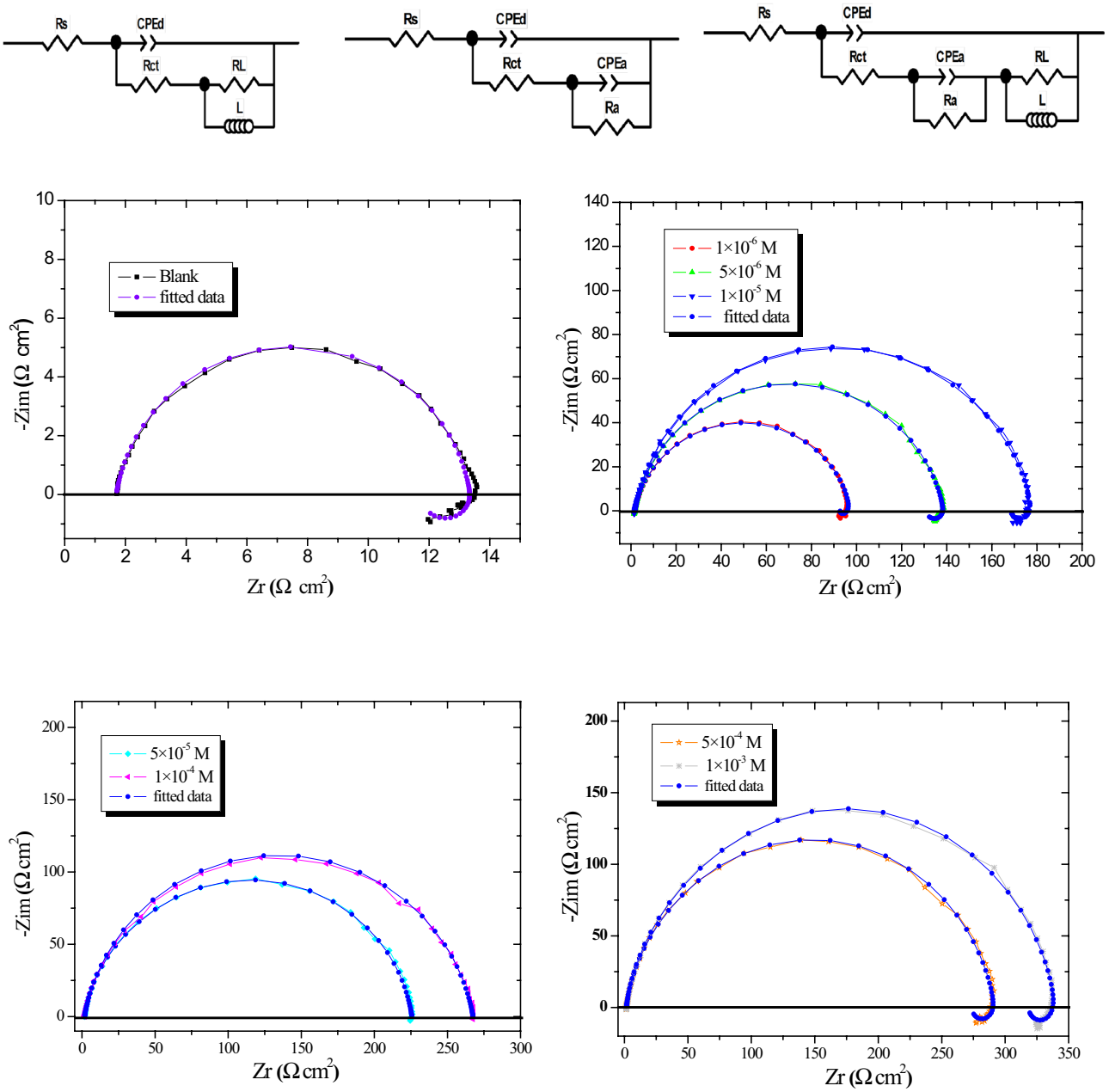

Fig. 6 Electrical equivalent circuits used to obtain the impedance parameters and comparison of experimental EIS data measured for mild steel in the absence and presence of various concentrations of inhibitor in 1.0 M HCl and the fitted data

that the interface behaves nearly capacitive [62]. The time constants τ_d are almost dependent for the concentration of inhibitor, while show a marked tendency to increase with concentration and its values are much higher than in the uninhibited acidic solutions which means slow adsorption process [59, 63].

It can be seen that the LF inductive loop disappears for the concentration 0.05 and 0.1 mM of inhibitor, for the others concentration of inhibitor we can observe an increase in the diameter of LF inductive loop with a concentration of P4E4P. Indeed the values of R_L increase and the values of inductance L are almost independent of the concentration.

For the concentration superior to 5×10^{-5} M, a two time constant can be used to describe the electrochemical impedance spectra in the presence of inhibitor. From the data in Table 3, it can be seen that the values of R_a increase with the concentration of inhibitor, but these values are lower than R_{ct}, so the polarization resistance R_p is dominated by R_{ct}. The values of n_a are lower that of n_d, indicating greater energy dissipation in the adsorption layer [64]. The values

Table 3 Impedance parameters and inhibition efficiency values for mild steel in 1.0 M HCl containing different concentrations of P4E4P at 308 K

C_{inh} (M)	R_s (Ω cm^2)	$10^6 A_d$ (Ω^{-1} s^n cm^{-2})	n_d	R_{ct} (Ω cm^2)	C_{dl} (μF cm^{-2})	τ_d (ms)	R_L (Ω cm^2)	L (H cm^{-2})	$10^6 A_a$ (Ω^{-1} s^n cm^{-2})	n_a	R_a (Ω cm^2)	C_a (μF cm^{-2})	τ_a (ms)	R_p (Ω cm^2)	η_Z (%)
Blank	1.705	385.69	0.906	10.03	217.34	2.18	1.63	12.72	–	–	–	–	–	11.7	–
1×10^{-6}	1.68	122.49	0.883	91.09	67.51	6.15	4.91	3.40	–	–	–	–	–	96.0	87.8
5×10^{-6}	1.71	94.12	0.89	129.3	54.58	7.06	6.41	27.89	–	–	–	–	–	135.7	91.3
1×10^{-5}	1.74	76.37	0.892	167.0	45.04	7.52	9.01	25.28	–	–	–	–	–	176.0	93.3
5×10^{-5}	1.78	53.24	0.924	157.2	35.92	5.65	–	–	144.95	0.83	66.72	57.19	3.82	223.9	94.8
1×10^{-4}	1.81	55.72	0.913	175.7	35.86	6.30	–	–	156.49	0.76	91.08	40.88	3.72	266.8	95.6
5×10^{-4}	1.73	46.80	0.919	184.7	30.79	5.69	18.62	88.05	220.00	0.78	87.4	72.18	6.31	290.7	95.7
1×10^{-3}	1.66	43.90	0919	200.0	28.92	5.78	21.84	72.36	128.82	0.80	117.1	45.15	5.29	338.9	96.5

Table 4 Effect of P4E4P concentration on corrosion data of steel in 1.0 M HCl

Inhibitor	Conc (M)	ν (mg/cm^2 h)	η_{WL}(%)
Blank	1.0	2.030	—
P4E4P	1×10^{-6}	0.167	91.7
	5×10^{-6}	0.143	92.9
	1×10^{-5}	0.140	93.1
	5×10^{-5}	0.105	94.8
	1×10^{-4}	0.085	95.8
	5×10^{-4}	0.078	96.1
	1×10^{-3}	0.055	97.3

of A_a, C_a, and τ_a are almost independent of the concentration of the inhibitor.

The related inhibition efficiency, η_Z (%), is calculated using Eq. (15) and listed in Table 3. It is clear that the increase in inhibitor concentration enhances R_p, and consequently increase the inhibition efficiency to reach their maximum value at 1×10^{-3} M ($R_p = 338.94\ \Omega\ cm^2$, η_Z (%) = 96.5) The inhibition efficiency calculated by EIS show the same trend as those obtained from the potentiodynamic polarization methods.

3.3 Gravimetric Measurements

3.3.1 Effect of Inhibitor Concentration

The values of the corrosion rate in the absence and presence of various concentrations of P4E4P at 308 K are given in Table 4. The fractional surface coverage θ can be easily determined from the weight loss measurements by the ratio η_{WL}(%)/100, where η_{WL}(%) is inhibition efficiency and calculated using relation 2. The data obtained suggest that the P4E4P get adsorbed on the mild steel surface at studied concentrations and corrosion rates decrease with increased concentration of inhibitor. This behavior could be attributed to the increase in adsorption of P4E4P at the metal/solution interface on increasing its concentration. Indeed, the adsorption of the P4E4P could occur due to the formation of links between the d-orbital of iron atoms, involving the displacement of water molecules from the metal surface, and the lone sp2 electron pairs present on the N, S and/or O atoms [65]. The order of the inhibition efficiency from the weight loss measurements are in good agreement with those obtained from the EIS and potentiodynamic polarization methods.

3.3.2 Effect of Temperature

In order to study the effect of temperature on the inhibition efficiency of inhibitor, Gravimetric measurements were carried

out in the temperature range 308–353 K in the absence and presence of 5×10^{-5}, 1×10^{-4}, 5×10^{-4}, and 1×10^{-3} M of inhibitor after 2 h of immersion time. The results obtained are summarized in Table 5. In hydrochloric acid media, dissolution of metal is generally accompanied with the evolution of hydrogen gas and the rise of temperature usually accelerates the corrosion reactions, resulting in a higher dissolution rate of the metal [66]. The data obtained in Table 5 show that the corrosion rate increased with increasing temperature in an uninhibited and inhibited solution, the increase in corrosion rate can be attributed to an appreciable decrease in the adsorption of the inhibitor in the mild steel surface with an increase in temperature. As adsorption decreases more desorption of inhibitor molecules occurs because these two opposite processes are in equilibrium. Due to more desorption of inhibitor molecules at higher temperatures the greater surface area of mild steel comes in contact with the acid environment, resulting in increased corrosion rates with an increase in temperature [67]. It was observed that the inhibition efficiency is almost constant and was decreased from 97.3 to 87.5% in the presence of 5×10^{-5}, 1×10^{-4}, 5×10^{-4}, and 1×10^{-3} M of inhibitor in the temperature range studied. This behavior led to the conclusion that a protective film of this compound formed on the mild steel surface is thermally stable in the temperature range studied [68].

3.3.3 Activation Parameters

Temperature can affect mild steel corrosion in acidic media in the presence and absence of inhibitor. To determine the activation energy of the corrosion process, weight loss measurements were taken at various temperatures (308–353 K) in the presence and absence of P4E4P. The corresponding results are also given in Table 5.

Figure 7 shows Arrhenius plots for the mild steel in 1.0 M HCl solutions in the absence and presence of P4E4P. The activation energies (E_a) can be expressed by the Arrhenius equation:

$$\nu = A\exp\left(-\frac{E_a}{RT}\right) \tag{16}$$

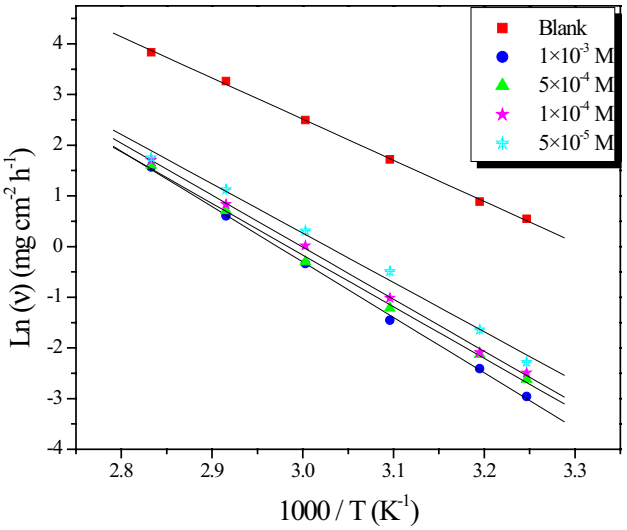

Fig. 7 Arrhenius plots of Ln (ν) versus $1/T$ for steel in 1.0 M HCl in the absence and the presence of P4E4P at different concentrations

where E_a is the apparent activation energy; A is the pre-exponential factor; T is the absolute temperature; R is the universal gas constant.

The plots of Ln (ν) against $1/T$ for mild steel in 1.0 M HCl in the absence and presence of different concentrations of P4E4P are shown in Fig. 7. From the Arrhenius equation and plots, values of activation energy can be obtained using the slopes and intercepts of the regression lines.

The process of adsorption between the metal surface and the inhibitor can sometimes be an exothermic process where the heat is given off, although in some cases, the endothermic process is encountered. The higher activation energy values indicate physical adsorption mechanism while the lower ones attribute for chemical adsorption mechanism [69]. The calculated activation energies, E_a, at different concentrations of the inhibitor are collected in Table 6. However, in our study, E_a increases with increasing the P4E4P concentration, and all values of E_a were higher than that in the absence of P4E4P. This type of inhibitor retards corrosion at ordinary temperatures but

Table 5 Effect of temperature on the corrosion rate of mild steel in 1.0 M HCl at different concentrations in the temperature range 308–353 K at 2 h

C_{inh} (M)	Blank	5×10^{-5}		1×10^{-4}		5×10^{-4}		1×10^{-3}	
Temp. (K)	ν^a_{corr}	ν^a_{corr}	η_{WL}	ν^a_{corr}	η_{WL}	ν^a_{corr}	η_{WL}	ν^a_{corr}	η_{WL}
308	1.73	0.121	93.0	0.081	95.3	0.087	95.5	0.055	96.8
313	2.43	0.194	92.0	0.124	94.9	0.119	95.1	0.090	96.3
323	5.58	0.614	89.0	0.363	93.5	0.296	94.7	0.234	95.8
333	12.11	1.368	88.7	1.017	91.6	0.739	93.9	0.714	94.1
343	26.11	3.081	88.2	2.298	91.2	2.036	92.2	1.828	93.0
353	46.23	5.779	87.5	5.501	88.1	4.993	89.2	4.808	89.6

[a]mg cm^{-2} h^{-1}

Table 6 The values of activation parameters for steel in 1.0 M HCl in the absence and the presence of different concentrations of P4E4P

C (M)	Linear regression coefficient	E_a (kJ/mol)	ΔH_a (kJ/mol)	ΔS_a (J/mol K)	$E_a - \Delta H_a$ (kJ/mol)
Blank	0.99948	67.50	64.77	−30.62	2.73
1×10^{-3}	0.99951	90.87	88.14	16.04	2.73
5×10^{-4}	0.99902	84.72	81.99	−1.27	2.73
1×10^{-4}	0.99952	85.37	82.64	−1.96	2.73
5×10^{-5}	0.99673	80.94	78.21	−9.01	2.73

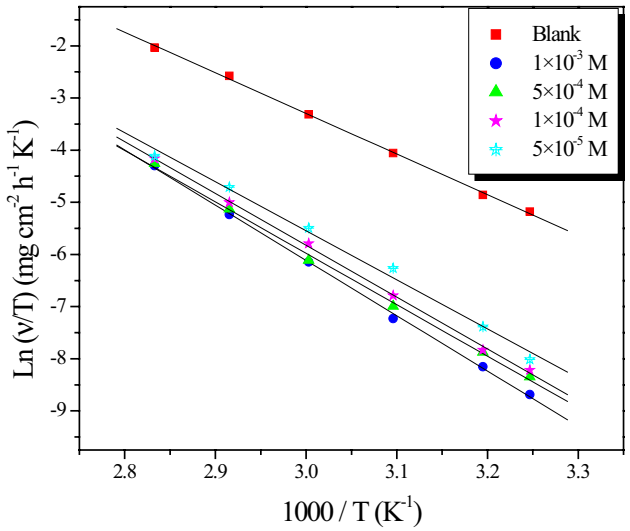

Fig. 8 Arrhenius plots of Ln (ν/T) versus $1/T$ for steel in 1.0 M HCl in the absence and the presence of P4E4P at different concentrations

inhibition is diminished at elevated temperature. Arrhenius law predicts that corrosion rate increases with the temperature and E_a may vary with temperature (Eq. 16).

The enthalpy of activation, ΔH_a, and entropy of activation ΔS_a were obtained from the Eyring transition state equation:

$$\nu = \frac{RT}{Nh}\exp\left(\frac{\Delta S_a}{R}\right)\exp\left(-\frac{\Delta H_a}{RT}\right) \quad (17)$$

where ν is the corrosion rate; h is the Planck's constant (6.626176×10^{-34} Js); N is the Avogadro's number (6.02252×10^{23} mol^{-1}); R is the universal gas constant; T is the absolute temperature; ΔH_a is the enthalpy of activation, and ΔS_a is the entropy of activation. Figure 8 shows a plot of Ln(ν/T) against $1/T$. Straight lines were obtained with a slope is equal to ($\Delta H_a/R$) and the intercept is equal to (Ln ($R/Nh + \Delta S_a/R$)), from which the values of ΔH_a and ΔS_a were calculated and listed in Table 6.

Examination of these data reveals that the values of ΔH_a and ΔS_a in the presence of the additives increase over that of the uninhibited solution. This implies that the energy barrier of the corrosion reaction in the presence of P4E4P increases which is expected. In the presence of the inhibitor, the value of ΔS_a increases and is generally interpreted as an increase in disorder as the reactants are converted to the activated complexes [70]. The positive sign of the enthalpy (ΔH_a) reflects the endothermic nature of the mild steel dissolution process (Table 6). This result permits to verify the known thermodynamic relation between E_a and ΔH_a as shown [71] also in Table 6:

$$E_a - \Delta H_a = RT \quad (18)$$

The calculated values are too close to RT is 2.73 kJ/mol. This result shows the inhibitor acted equally on E_a and ΔH_a.

3.3.4 Adsorption Parameters

The values of surface coverage θ corresponding to different concentrations of P4E4P in the temperature range from 308 to 353 K have been used to explain the best isotherm to determine the adsorption process. The fractional surface coverage θ can be easily determined from weight loss measurements by the ratio $\eta_{WL}(\%)/100$ (Table 5), if one assumes that the values of $\eta_{WL}(\%)$ do not differ substantially from surface coverage (θ). As it is known that the adsorption of an organic adsorbate onto metal-solution interface can be presented as a substitutional adsorption process between the organic molecules in the aqueous solution $Org_{(sol)}$ and the water molecules on the metallic surface $H_2O_{(ads)}$:

$$Org_{(sol)} + nH_2O_{(ads)} \ll Org_{(ads)} + nH_2O_{(sol)} \quad (19)$$

where $Org_{(sol)}$ and $Org_{(ads)}$ are the organic molecules in the aqueous solution and adsorbed on the metallic surface, respectively; $H_2O_{(ads)}$ is the water molecules on the metallic surface; n is the size ratio representing the number of water molecules replaced by one molecule of organic adsorbate. When the equilibrium of the process described in this equation is reached, it is possible to obtain different expressions of the adsorption isotherm plots, and thus the surface coverage degree (θ) can be plotted as a function of the concentration of the inhibitor under test [72]. The Langmuir adsorption isotherm was found to give the best description of the adsorption behavior of P4E4P. In this case, the surface coverage (θ) of the inhibitor on the steel surface is related

to the concentration of inhibitor in the solution according to the following equation:

$$\frac{\theta}{1-\theta} = K_{ads} C_{inh} \tag{20}$$

Rearranging this equation gives

$$\frac{C_{inh}}{\theta} = \frac{1}{K_{ads}} + C_{inh} \tag{21}$$

where θ is the surface coverage degree; C_{inh} is the inhibitor concentration in the electrolyte, and K_{ads} is the equilibrium constant of the adsorption process. The K_{ads} values may be taken as a measure of the strength of the adsorption forces between the inhibitor molecules and the metal surface [73]. To calculate the adsorption parameters, the straight lines were drawn using the least squares method. The experimental (points) and calculated isotherms (lines) are plotted in Fig. 9. The results are presented in Table 7. A very good fit is observed with a regression coefficient (R^2) up to 0.9999 and the obtained lines have slopes very close to unity, which suggests that the experimental data are well described by Langmuir isotherm and exhibit single-layer adsorption characteristic [74]. This kind of isotherm involves the assumption of no interaction between the adsorbed species and the electrode surface. From the intercepts of the straight lines C_{inh}/θ—axis, the K_{ads} values were calculated and given in Table 7.

The obtained values of K_{ads} are related to the standard free energy of adsorption (ΔG°_{ads}) according to the expression in Eq. 22 [75]:

$$K_{ads} = \frac{1}{55.5} \exp\left[\frac{-\Delta G^{\circ}_{ads}}{RT}\right] \tag{22}$$

Equation 22 can also rearrange to

$$\Delta G^{\circ}_{ads} = -RTLn\left(55.5 K_{ads}\right) \tag{23}$$

A thermodynamic model is very useful to explain the adsorption phenomenon of inhibitor molecule. The adsorption heat could be calculated according to the Van't Hoff equation [72, 76]:

$$\mathrm{Ln}\left(K_{ads}\right) = -\frac{\Delta H^{\circ}_{ads}}{RT} + \text{constant} \tag{24}$$

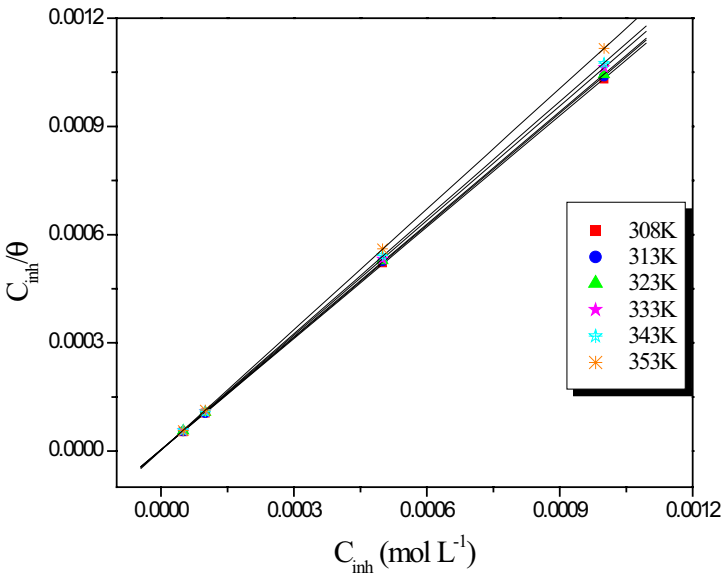

Fig. 9 Langmuir's isotherm adsorption model of P4E4P on the mild steel surface in 1.0 M HCl at different temperatures

Table 7 Thermodynamic parameters of adsorption of P4E4P on the mild steel surface at different temperatures

Temp (K)	Linear regression coefficient	Slope	K_{ads} (L/mol)	ΔG°_{ads} (kJ/mol)	ΔH°_{ads} (kJ/mol)	ΔS°_{ads}(J/mol K)
308	0.99998	1.02	340345.58	−42.90	−4.817	123.65
313	0.99998	1.03	314053.58	−43.39		123.24
323	0.99999	1.04	312134.70	−44.75		123.63
333	1.00000	1.06	310524.29	−46.13		124.06
343	0.99999	1.07	297534.04	−47.39		124.12
353	1.00000	1.11	247194.34	−48.23		122.98

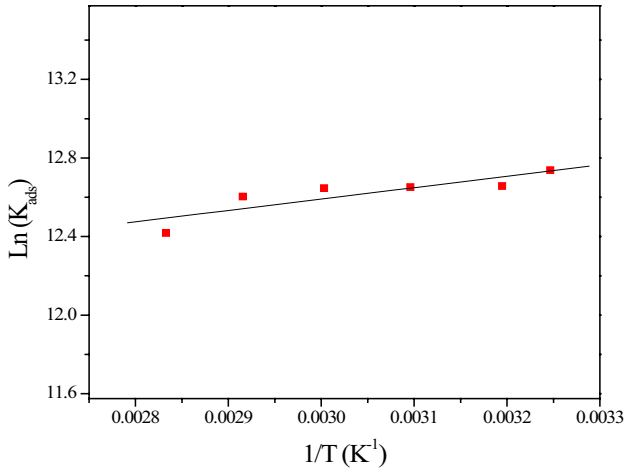

Fig. 10 The relationship between Ln (K_{ads}) and 1/T for mild steel in 1.0 M HCl solution containing different concentrations of P4E4P

where ΔG°_{ads} and K_{ads} are the adsorption heat and adsorptive equilibrium constant, respectively.

To obtain the adsorption heat, the regression between(K_{ads}) and 1/T was dealt with. Figure 10 is the straight line Ln(K_{ads}) versus 1/T. The adsorption heat (ΔH) can be approximately regarded as the standard adsorption heat (ΔH°_{ads}) under the experimental conditions [75, 77].

The negative value of ΔG°_{ads} (Table 7) means that the adsorption of P4E4P on mild steel surface is a spontaneous process, and furthermore the negative values of ΔG°_{ads} also show the strong interaction of the inhibitor molecule onto the mild steel surface [78, 79].

Generally, values of ΔG°_{ads} around -20 kJ mol^{-1} or lower are consistent with the electrostatic interaction between the charged molecules and the charged metal (physisorption). Those more negative than -40 kJ mol^{-1} involve charge sharing or transfer from the inhibitor molecules to the metal surface to form a coordinate type of bond (chemisorption) [80, 81]. The obtained ΔG^{o}_{ads} values in the studied temperature domain are in the range of -48.23 to -42.90 kJ mol^{-1}, indicating, therefore that the adsorption mechanism of the P4E4P onto mild steel in1.0 M HCl solution is mainly due to chemisorption (Table 7). On the other hand, the obtained values of ΔG°_{ads} generally show a regular dependence on temperature, indicating a good correlation among thermodynamic parameters. The negative value of ΔH°_{ads} also shows that the adsorption of inhibitor is an exothermic process [82]. Generally, an exothermic process signifies either physical or chemisorption while the endothermic process is attributable unequivocally to chemisorption [83]. In an exothermic process, physisorption is distinguished from chemisorption by considering the absolute value of a physisorption process is lower than 40 kJ mol^{-1} while the adsorption heat of a chemisorption process approaches 100 kJ mol^{-1} [84]. In the present case, the standard adsorption heat -4.817 kJ mol^{-1} shows that a comprehensive adsorption (physical adsorption) might occur [72]. $\Delta H^{\circ}_{ads} = -4.817$ kJ mol^{-1} found by the Van't Hoff equation may be also evaluated by the Gibbs-Helmholtz equation, which is defined as follows:

$$\left[\frac{\partial(\Delta G^{\circ}_{ads}/T)}{\partial T}\right]_{P} = -\frac{\Delta H^{\circ}_{ads}}{T^{2}} \tag{25}$$

which can be arranged to give the following equation:

$$\frac{\Delta G^{\circ}_{ads}}{T} = \frac{\Delta H^{\circ}_{ads}}{T} + A \tag{26}$$

The standard adsorption entropy ΔS°_{ads} may be deduced using the thermodynamic basic equation:

$$\Delta G^{\circ}_{ads} = \Delta H^{\circ}_{ads} - T\Delta S^{\circ}_{ads} \tag{27}$$

The variation of $\Delta G^{\circ}_{ads}/T$ with 1/T gives a straight line with a slope that equals $\Delta H^{\circ}_{ads} = -4.819$ KJ mol^{-1} (Fig. 11). It can be seen from the figure that $\Delta G^{\circ}_{ads}/T$ decreases with 1/T. The value of the enthalpy of adsorption found by the two methods such as Van't Hoff and Gibbs–Helmholtz relations is in good agreement.

The values of ΔS°_{ads} are positive in the adsorption process indicating an increase in solvent entropy [85]. The positive values of ΔS°_{ads} suggest that the adsorption is coupled with an increase in the system disorder due to the adsorption of the inhibitor on the mild steel surface [86].

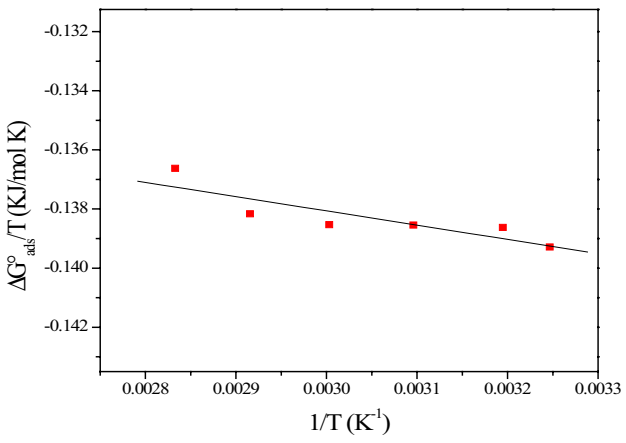

Fig. 11 Relationship between $\Delta G^{\circ}_{ads}/T$ and the reverse of absolute temperature

3.4 Computational Procedures

Quantum chemical calculations were done in order to discuss the adsorption mode through light on the inhibitor molecular structure. It is well known that the *N*-heterocyclic compound could be protonated in the acid solution. According to some quantum chemical studies about protonated *N*-heterocyclic inhibitor in HCl solution [87], the proton affinity is clearly favored toward the hetero N atom of *N*-heterocyclic ring. The calculated value of protonated affiliation energy (PA) confirms that P4E4P is easily protonated by H^+.

Figure 12 shows the optimized molecular structures of neutral and protonated P4E4P. It is well known that organic inhibitor can form coordination bonds between the unshared electron pairs of O, N, or S atom and the empty p-orbitals of Fe atom. The larger negative charge of the atom, the better is the action as an electronic donor. Mulliken charges of the atoms are listed in Table 8. By careful examination of the values of Mulliken charges, the larger negative atoms are found in N1, N19, and O42, which are active adsorptive centers. For protonated P4E4P, the Mulliken charge of O42 becomes more negative than N1 and N19. This result implies that if the inhibitor is protonated, O42 exhibits more active than N1 and N19. But the difference between the two protonated and non-protonated forms is more superior in the case of N19, this result is confirmed by the calculation of PA, and hence the preferred site for protonation is the N19 atom.

The optimized geometries of the P4E4P and p-P4E4P including their HOMO and LUMO distribution density were in Fig. 13. The distribution HOMO is mainly localized on a (ethylthio) ethyl, but the LUMO distribution is mainly located on a pyridine ring.

In Table 9, the calculated E_{HOMO}, E_{LUMO}, ΔE, χ, η, and μ were given. The results obtained from different quantum chemical calculation methods showed the same trend.

The theory of frontier molecular orbital theory suggests that the formation of a transition state is due to an interaction between HOMO and LUMO orbitals of reacting species [88]. The E_{HOMO} energy is associated with electron donating ability of the molecule. The high E_{HOMO} proves that the molecule has a trend to donate electrons to an acceptor molecule's LUMO orbital [89–91]. In Table 9, all E_{HOMO} values were negative. Arslan et al. [92] suggested that the negative E_{HOMO} values were evidence of physical adsorption. The low E_{LUMO} value indicates that the electron accepting ability of the molecule is very high [23, 93]. The p-P4E4P has lower E_{LUMO} than P4E4P (Table 9). The ΔE values suggest that

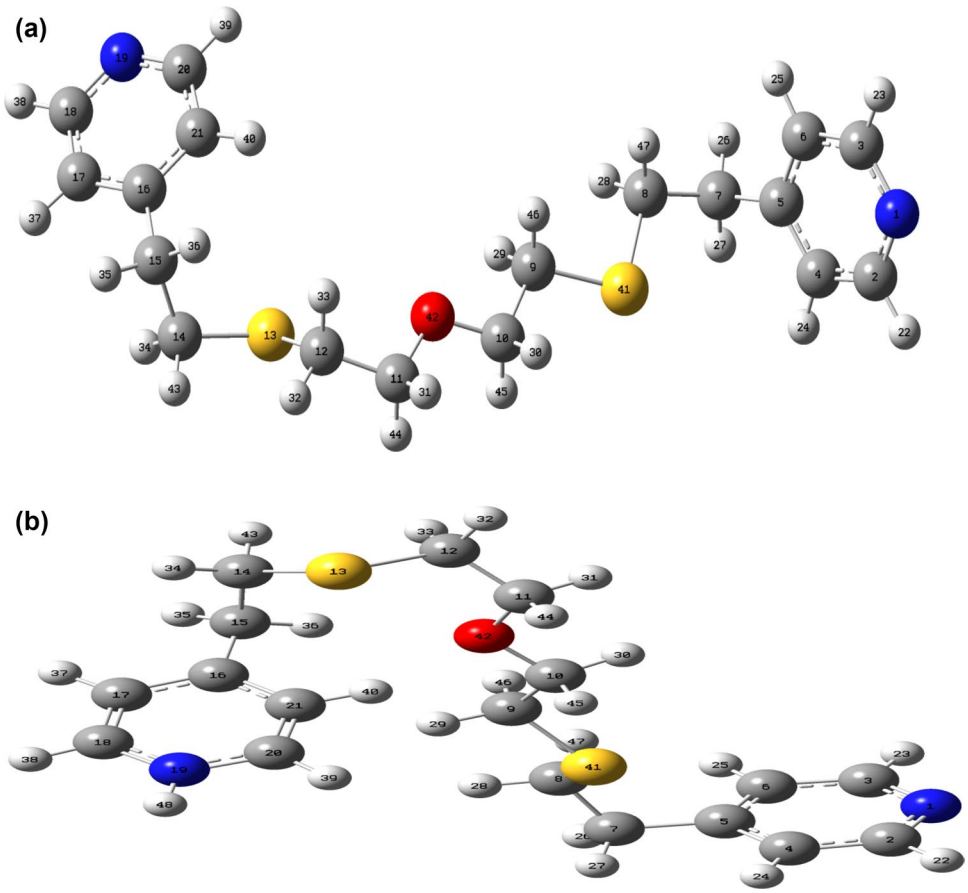

Fig. 12 Optimized molecular structures of the neutral and protonated P4E4P: **a** P4E4P; **b** p-P4E4P

Table 8 Quantum chemical parameters of Mulliken charge, for neutral and protonated P4E4P molecules

Atom	Mulliken charge	
	P4E4P	p-P4E4P
1 N	−0.432847	−0.424657
2 C	0.094717	0.097332
3 C	0.094206	0.096079
4 C	−0.118990	−0.122046
5 C	0.151858	0.149608
6 C	−0.125452	−0.127236
7 C	−0.267351	−0.268219
8 C	−0.314405	−0.319863
9 C	−0.347456	−0.354977
10 C	0.074806	0.059069
11 C	0.074139	0.077442
12 C	−0.343136	−0.371196
13 S	0.107758	0.111164
14 C	−0.334930	−0.351258
15 C	−0.244852	−0.263540
16 C	0.145780	0.163026
17 C	−0.127930	−0.137557
18 C	0.093626	0.169811
19 N	−0.433067	−0.482443
20 C	0.090359	0.162818
21 C	−0.107570	−0.106054
41 S	0.085530	0.101416
42 O	−0.491016	−0.512461

the neutral species is also more reactive than the protonated species. It is, therefore, reasonable to infer that the protonated species of metronidazole are less likely to interact with the metal surface as compared to the neutral species. The higher μ for p-P4E4P in comparison to P4E4P showed that the dipole–dipole interaction of p-P4E4P and metal surface higher.

4 Conclusions

The inhibition of 4-(2-(2-(2-(2-(pyridine-4-yl)ethylthio) ethoxy)ethylthio)ethyl)pyridine (P4E4P) for the corrosion of mild steel in 1.0 M HCl solution was evaluated by experimental measurements and theoretical calculations. P4E4P exhibits good inhibition property and its efficacy increases with the increasing inhibitor concentrations. However, the increase in temperature obviously decreases the protection efficiency of the additive. Potentiodynamic polarization tests indicate that P4E4P acts as a mixed-type inhibitor. The adsorption process accords with the Langmuir adsorption model. EIS curves imply that inhibitor increases the charge transfer resistances and leads to a decrease in the double-layer value, suggesting that inhibitor acts through the adsorption on the steel surface. Data obtained from quantum chemical calculations using DFT at the B3LYP/6-31G level of theory were correlated to the

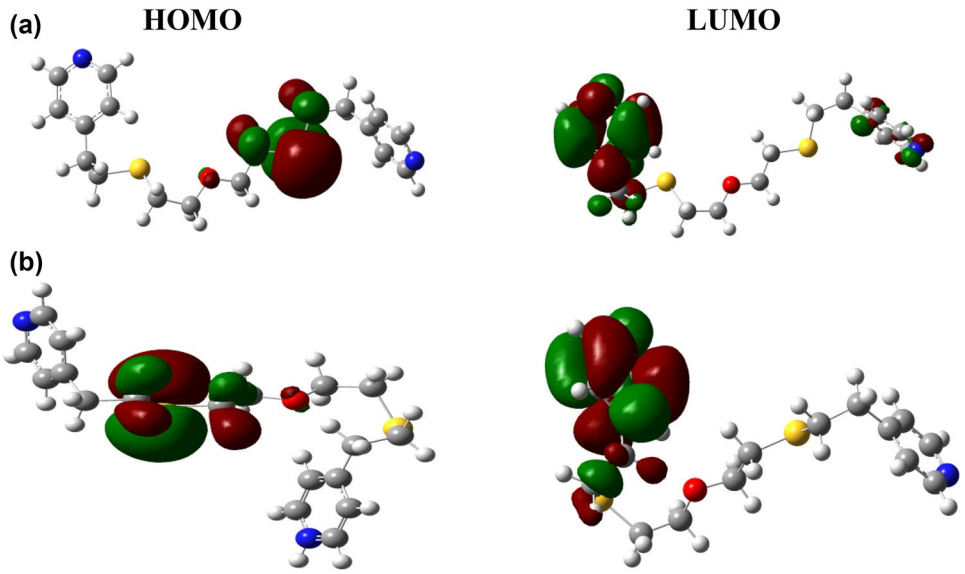

Fig. 13 The HOMO and LUMO orbitals of optimized P4E4P (**a**) and p-P4E4P (**b**) molecules

Table 9 The calculated quantum chemical parameters for the neutral and protonated species of P4E4P

Molecule	E_{HOMO} (eV)	E_{LUMO} (eV)	ΔE (eV)	χ	η	μ (Debye)
Neutral species	−6.0660	−0.5992	5.4668	−3.3326	2.7334	3.0222
Protonated species	−8.2595	−6.14846	2.1111	−7.2040	1.0555	4.8300

inhibitive effect of P4E4P. Both experimental and theoretical calculations are in agreement.

References

1. Schmitt G (1984) Application of inhibitors for acid media: report prepared for the European federation of corrosion working party on inhibitors. Br Corros J 19(4):165–176
2. Bendaha H, Zarrouk A, Aouniti A, Hammouti B, El Kadiri S, Salghi R, Touzani R (2012) Adsorption and corrosion inhibitive properties of some tripodal pyrazolic compounds on mild steel in hydrochloric acid systems. Phys Chem News 64:95–103
3. Ghazoui A, Bencaht N, Al-Deyab SS, Zarrouk A, Hammouti B, Ramdani M, Guenbour M (2013) An investigation of two novel pyridazine derivatives as corrosion inhibitor for C38 steel in 1.0 M HCl. Int J Electrochem Sci 8:2272–2292
4. Zarrouk A, Zarrok H, Salghi R, Bouroumane N, Hammouti B, Al-Deyab SS, Touzani R (2012) The adsorption and corrosion inhibition of 2-[bis-(3,5-dimethyl-pyrazol-1-ylmethyl)-amino]-pentanedioic acid on carbon steel corrosion in 1.0 m HCl. Int J Electrochem Sci 7:10215–10232
5. Zarrok H, Zarrouk A, Salghi R, Ramli Y, Hammouti B, Assouag M, Essassi EM, Oudda H, Taleb M (2012) 3,7-Dimethylquinoxalin-2-(1H)-one for inhibition of acid corrosion of carbon steel. J Chem Pharm Res 4(12):5048–5055
6. Zarrouk A, Hammouti B, Zarrok H, Bouachrine M, Khaled KF, Al-Deyab SS (2012) Corrosion inhibition of copper in nitric acid solutions using a new triazole derivative. Int J Electrochem Sci 7:89–105
7. Ghazoui A, Saddik R, Benchat N, Guenbour M, Hammouti B, Al-Deyab SS, Zarrouk A (2012) Comparative study of pyridine and pyrimidine derivatives as corrosion inhibitors of C38 steel in molar HCl. Int J Electrochem Sci 7:7080–7097
8. Zarrok H, Al Mamari K, Zarrouk A, Salghi R, Hammouti B, Al-Deyab SS, Essassi EM, Bentiss F, Oudda H (2012) Gravimetric and electrochemical evaluation of 1-allyl-1hindole-2,3-dione of carbon steel corrosion in hydrochloric acid. Int J Electrochem Sci 7:10338–10357
9. Zarrouk A, Hammouti B, Dafali A, Bentiss F (2013) Inhibitive properties and adsorption of purpald as a corrosion inhibitor for copper in nitric acid medium. Ind Eng Chem Res 52(7):2560–2568
10. Zarrok H, Oudda H, El Midaoui A, Zarrouk A, Hammouti B, Touhami ME, Attayibat A, Radi S, Touzani R (2012) ome new bipyrazole derivatives as corrosion inhibitors for C38 steel in acidic medium. Res Chem Intermed 38(8):2051–2063
11. Solmaz R, Altunbas E, Kardas G (2011) Investigation of adsorption and corrosion inhibition effect of 1,1'-thiocarbonyldiimidazole on mild steel in hydrochloric acid solution. Prot Met Phys Chem Sur 47(2):264–271
12. Solmaz R, Mert ME, Kardas G, Yazici B, Erbil M (2008) Adsorption and corrosion inhibition effect of 1,1'-thiocarbonyldiimidazole on mild steel in H2SO4 solution and synergistic effect of iodide ion. Acta Phys Chim Sin 24(7):1185–1191
13. Belayachi M, Serrar H, Zarrok H, El Assyry A, Zarrouk A, Oudda H, Boukhris S, Hammouti B, Ebenso EE, Geunbour A (2015) New pyrimidothiazine derivative as corrosion inhibitor for carbon steel in acidic media. Int J Electrochem Sci 10:3010–3025
14. Caliskan N, Akbas E (2012) Contribution to adsorption of aromatic amines on mild steel surface from HCl solutions by impedance, UV, and Raman spectroscopy. Mater Corros 63(3):231–237
15. Abd El-Maksoud SA, Fouda AS (2005) Some pyridine derivatives as corrosion inhibitors for carbon steel in acidic medium. Mater Chem Phys 93(1):84–90
16. Quraishi MA, Sharma HK (2002) 4-Amino-3-butyl-5-mercapto-1,2,4-triazole: a new corrosion inhibitor for mild steel in sulphuric acid. Mater Chem Phys 78(1):18–21
17. Ansari KR, Quraishi MA, Singh A (2014) Schiff's base of pyridyl substituted triazoles as new and effective corrosion inhibitors for mild steel in hydrochloric acid solution. Corros Sci 79:5–15
18. Kosari A, Moayed MH, Davoodi A, Parvizi R, Momeni M, Eshghi H, Moradi H (2014) Electrochemical and quantum chemical assessment of two organic compounds from pyridine derivatives as corrosion inhibitors for mild steel in HCl solution under stagnant condition and hydrodynamic flow. Corros Sci 78:138–150
19. Bentiss F, Outirite M, Traisnel M, Vezin H, Lagrenée M, Hammouti B, Al-Deyab SS, Jama C (2012) Improvement of corrosion resistance of carbon steel in hydrochloric acid medium by 3,6-bis(3-pyridyl)pyridazine. Int J Electrochem Sci 7:1699–1723
20. Elbakri M, Touir R, Touhami ME, Zarrouk A, Aouine Y, Sfaira M, Bouachrine M, Alami A, El Hallaoui A (2013) Inhibiting effects of benzamide derivatives on the corrosion of mild steel in hydrochloric acid solution. Res Chem Intermed 39(6):2417–2433
21. Tu S, Jiang X, Zhou L, Duan M, Wang H, Jiang X (2012) Synthesis of N-alkyl-4-(4-hydroxybut-2-ynyl) pyridinium bromides and their corrosion inhibition activities on X70 steel in 5 M HCl. Corros Sci 65:13–25
22. Zhang F, Tang Y, Cao Z, Jing W, Wu Z, Chen Y (2012) Performance and theoretical study on corrosion inhibition of 2-(4-pyridyl)-benzimidazole for mild steel in hydrochloric acid. Corros Sci 61:1–9
23. Gece G (2008) The use of quantum chemical methods in corrosion inhibitor studies. Corros Sci 50(11):2981–2992
24. Torres VV, Rayol VA, Magalhaes M, Viana GM, Aguiar LCS, Machado SP, Orofino H, D'Elia E (2014) Study of thioureas derivatives synthesized from a green route as corrosion inhibitors for mild steel in HCl solution. Corros Sci 79:108–118
25. Issaadi S, Douadi T, Chafaa S (2014) Adsorption and inhibitive properties of a new heterocyclic furan Schiff base on corrosion of copper in HCl 1 M: experimental and theoretical investigation. Appl Surf Sci 316:582–589
26. Zarrok H, Zarrouk A, Salghi R, Touhami ME, Oudda H, Hammouti B, Touir R, Bentiss F, Al-Deyab SS (2013) Corrosion inhibition of C38 steel in acidic medium using N-1 naphthylethylenediamine dihydrochloride monomethanolate. Int J Electrochem Sci 8:6014–6032
27. Ma H, Chen S, Liu Z, Sun Y (2006) Theoretical elucidation on the inhibition mechanism of pyridine–pyrazole compound: a Hartree Fock study. J Mol Struct (THEOCHEM) 774(1–3):19–22
28. Henríquez-Román JH, Padilla-Campos L, Páez MA, Zagal JH, María Rubio A, Rangel CM, Costamagna J, Cárdenas-Jirón G (2005) The influence of aniline and its derivatives on the corrosion behaviour of copper in acid solution: a theoretical approach. J Mol Struct (THEOCHEM) 757(1–3):1–7
29. Rodrguez-Valdez LM, Martnez-Villafane A, Glossman-Mitnik D (2005) Computational simulation of the molecular structure and properties of heterocyclic organic compounds with possible corrosion inhibition properties. J Mol Struct (THEOCHEM) 713:65–70
30. Feng Y, Chen S, Guo W, Zhang Y, Liu G (2007) Inhibition of iron corrosion by 5,10,15,20-tetraphenylporphyrin and 5,10,15,20-tetra-(4-chlorophenyl)porphyrin adlayers in 0.5 M H2SO4 solutions. J Electroanal Chem 602(1):115–122
31. Frisch MJ, Trucks GW, Schlegel HB, Scuseria GE, Robb MA, Cheeseman JR, Montgomery JrJA., Vreven T, Kudin KN, Burant JC, Millam JM, Iyengar SS, Tomasi J, Barone V, Mennucci B, Cossi M, Scalmani G, Rega N, Petersson GA, Nakatsuji H, Hada M, Ehara M, Toyota K, Fukuda R, Hasegawa J,

Ishida M, Nakajima T, Honda Y, Kitao O, Nakai H, Klene M, Li X, Knox JE, Hratchian HP, Cross JB, Bakken V, Adamo C, Jaramillo J, Gomperts R, Stratman RE, Yazyev O, Austin AJ, Cammi R, Pomelli C, Ochterski JW, Ayala PY, Morokuma K, Voth GA, Salvador P, Dannenberg JJ, Zakrzewski VG, Dapprich S, Daniels AD, Strain MC, Farkas O, Malick DK, Rabuck AD, Raghavachari K, Foresman JB, Ortiz JV, Cui Q, Baboul AG, Clifford S, Cioslowski J, Stefanov BB, Liu G, Liashenko A, Piskorz P, Komaromi I, Martin RL, Fox DJ, Keith T, Al-Laham MA, Peng CY, Nanayakkara A, Challacombe M, Gill PMW, Johnson B, Chen W, Wong MW, Gonzalez C, Pople JA (2004) Gaussian 03, Revision E.01, Gaussian, Inc., Wallingford CT

32. Dewar MJS, Thiel W (1977) Ground states of molecules. 38. The MNDO method. Approximations and parameters. J Am Chem Soc 99(15):4899–4907
33. Pearson RG (1988) Absolute electronegativity and hardness: application to inorganic chemistry. Inorg Chem 27(4):734–740
34. Wang Z (2012) The inhibition effect of bis-benzimidazole compound for mild steel in 0.5 M HCl solution. Int J Electrochem Sci 7:11149–11160
35. Saliyan VR, Adhikari AV (2008) Quinolin-5-ylmethylene-3-{[8-(trifluoromethyl)quinolin-4-yl]thio}propanohydrazide as an effective inhibitor of mild steel corrosion in HCl solution. Corros Sci 50(1):55–61
36. Liu FG, Du M, Zhang J, Qiu M (2009) Electrochemical behavior of Q235 steel in saltwater saturated with carbon dioxide based on new imidazoline derivative inhibitor. Corros Sci 51(1):102–109
37. Krim O, Elidrissi A, Hammouti B, Ouslim A, Benkaddour M (2009) Synthesis, characterization, and comparative study of pyridine derivatives as corrosion inhibitors of mild steel in HCl medium. Chem Eng Comm 196:1536–1546
38. Bouklah M, Attayibat A, Hammouti B, Ramdani A, Radi S, Benkaddour M (2005) Pyridine–pyrazole compound as inhibitor for steel in 1M HCl. App Surf Sci 240:341–348
39. Tebbji K, Oudda H, Hammouti B, Benkaddour M, El Kodadi M, Ramdani A (2005) Inhibition effect of two organic compounds pyridine–pyrazole type in acidic corrosion of steel. Colloids Surf A Physicochem Eng Asp 259:143–149
40. Meng Y, Ning W, Xu B, Yang W, Zhang K, Chen Y, Li L, Liu X, Zhenga J, Zhang Y (2017) Inhibition of mild steel corrosion in hydrochloric acid using two novel pyridine Schiff base derivatives: a comparative study of experimental and theoretical results. RSC Adv 7:43014–43029
41. Amin MA, Abd El-Rehim SS, El-Sherbini EEF, Bayyomi RS (2007) The inhibition of low carbon steel corrosion in hydrochloric acid solutions by succinic acid: part I. Weight loss, polarization, EIS, PZC, EDX and SEM studies. Electrochim Acta 52(11):3588–3600
42. Lenderink HJW, Linden MVD, De Wit JHW (1993) Corrosion of aluminium in acidic and neutral solutions. Electrochim Acta 38(14):1989–1992
43. Amin MA, Khaled KF, Mohsen Q, Arida HA (2010) A study of the inhibition of iron corrosion in HCl solutions by some amino acids. Corros Sci 52(5):1684–1695
44. Kedam M, Mattos OR, Takenouti H (1981) Reaction model for iron dissolution studied by electrode impedance: I. Experimental results and reaction model. J Electrochem Soc 128(2):257–266
45. Veloz MA, Gonzalez I (2002) Electrochemical study of carbon steel corrosion in buffered acetic acid solutions with chlorides and H2S. Electrochim Acta 48(2):135–144
46. Lebrini M, Robert F, Lecante A, Roos C (2011) Corrosion inhibition of C38 steel in 1M hydrochloric acid medium by alkaloids extract from Oxandra asbeckii plant. Corros Sci 53(2):687–695
47. Morad MS (2000) An electrochemical study on the inhibiting action of some organic phosphonium compounds on the corrosion of mild steel in aerated acid solutions. Corros Sci 42(8):1307–1326
48. Sherif EM, Park SM (2006) Effects of 1,4-naphthoquinone on aluminum corrosion in 0.50M sodium chloride solutions. Electrochim Acta 51(7):1313–1321
49. Kelly EJ (1965) Iron dissolution and hydrogen evolution reactions in acidic sulfate solutions. J Electrochem Soc 112(2):124–131
50. Mahdavian M, Ashhari S (2010) Corrosion inhibition performance of 2-mercaptobenzimidazole and 2-mercaptobenzoxazole compounds for protection of mild steel in hydrochloric acid solution. Electrochim Acta 55(5):1720–1724
51. Xu B, Yang W, Liu Y, Yin X, Gong W, Chen Y (2014) Experimental and theoretical evaluation of two pyridinecarboxaldehyde thiosemicarbazone compounds as corrosion inhibitors for mild steel in hydrochloric acid solution. Corros Sci 78:260–268
52. Macdonald JR (1987) Impedance spectroscopy and its use in analyzing the steady-state AC response of solid and liquid electrolytes. Electroanal Chem 223(1–2):25–50
53. Behpour M, Ghroreishi SM, Soltani N, Salavati-Niasari M, Hamadanian M, Gandomi A (2008) Electrochemical and theoretical investigation on the corrosion inhibition of mild steel by thiosalicylaldehyde derivatives in hydrochloric acid solution. Corros Sci 50(8):2172–2181
54. Lopez DA, Simison SN, de Sanchez SR (2003) The influence of steel microstructure on CO_2 corrosion. EIS studies on the inhibition efficiency of benzimidazole. Electrochim Acta 48(7):845–854
55. Stoynov ZB, Grafov BM, Savova-Stoynova B, Elkin VV (1991) Electrochemical impedance. Nauka, Moscow
56. Musa AY, Kadhum AAH, Mohamad AB, Takriff MS (2010) Experimental and theoretical study on the inhibition performance of triazole compounds for mild steel corrosion. Corros Sci 52(10):3331–3340
57. Jacob KS, Parameswaran G (2010) Corrosion inhibition of mild steel in hydrochloric acid solution by Schiff base furoin thiosemicarbazone. Corros Sci 52(1):224–228
58. Labjar N, Lebrini M, Bentiss F, Chihib N, ElHajjaji S, Jama C (2010) Corrosion inhibition of carbon steel and antibacterial properties of aminotris-(methylenephosphonic) acid. Mater Chem Phys 119(1–2):330–336
59. Zheng X, Zhang S, Li W, Yin H, He J, Wua J (2014) Investigation of 1-butyl-3-methyl-1H-benzimidazolium iodide as inhibitor for mild steel in sulfuric acid solution. Corros Sci 80:383–392
60. Outirite M, Lagrenee M, Lebrini M, Traisnel M, Jama C, Vezin H, Bentiss F (2010) AC impedance, X-ray photoelectron spectroscopy and density functional theory studies of 3,5-bis(n-pyridyl)-1,2,4-oxadiazoles as efficient corrosion inhibitors for carbon steel surface in hydrochloric acid solution. Electrochim Acta 55(5):1670–1681
61. Growcock FB, Jasinski JH (1989) Time-resolved impedance spectroscopy of mild steel in concentrated hydrochloric acid. J Electrochem Soc 136(8):2310–2314
62. Morad MS (2008) Inhibition of iron corrosion in acid solutions by Cefatrexyl: behaviour near and at the corrosion potential. Corros Sci 50(2):436–448
63. Lebrini M, Bentiss F, Chihib N, Jama C, Hornez JP, Lagrenée M (2008) Polyphosphate derivatives of guanidine and urea copolymer: inhibiting corrosion effect of Armco iron in acid solution and antibacterial activity. Corros Sci 50(10):2914–2918
64. Popova A, Christov M, Vasilev A (2007) itive properties of quaternary ammonium bromides of N-containing heterocycles on acid mild steel corrosion. Part II: EIS results. Corros Sci 49(8):3290–3302
65. Zarrok H, Zarrouk A, Hammouti B, Salghi R, Jama C, Bentiss F (2012) Corrosion control of carbon steel in phosphoric acid by purpald—weight loss, electrochemical and XPS studies. Corros Sci 64:243–252

66. Yadav DK, Quraishi MA, Maiti B (2012) Inhibition effect of some benzylidenes on mild steel in 1 M HCl: an experimental and theoretical correlation. Corros Sci 55:254–266
67. Herrag L, Hammouti B, Elkadiri S, Aouniti A, Jama C, Vezin H, Bentiss F (2010) Adsorption properties and inhibition of mild steel corrosion in hydrochloric solution by some newly synthesized diamine derivatives: experimental and theoretical investigations. Corros Sci 52(9):3042–3051
68. Singh AK, Quraishi MA (2010) The effect of some bis-thiadiazole derivatives on the corrosion of mild steel in hydrochloric acid. Corros Sci 52(4):1373–1385
69. Bentiss F, Lebrini M, Lagrenée M (2005) Thermodynamic characterization of metal dissolution and inhibitor adsorption processes in mild steel/2,5-bis(n-thienyl)-1,3,4-thiadiazoles/hydrochloric acid system. Corros Sci 47(12):2915–2931
70. Ghazoui A, Saddik R, Benchat N, Hammouti B, Guenbour M, Zarrouk A, Ramdani M (2012) The role of 3-amino-2-phenylimidazo[1,2-a]pyridine as corrosion inhibitor for C38 steel in 1M HCl. Der Pharm Chem 4(1):352–364
71. Stern M, Geary AL (1957) Electrochemical polarization I. A theoretical analysis of the shape of polarization curves. J Electrochem Soc 104(1):56–63
72. Labjar N, Bentiss F, Lebrini M, Jama C, El hajjaji S (2011) Study of temperature effect on the corrosion inhibition of C38 carbon steel using amino-tris(methylenephosphonic) acid in hydrochloric acid solution. Int J Corros. https://doi.org/10.1155/2011/548528
73. Amin MA (2006) Weight loss, polarization, electrochemical impedance spectroscopy, SEM and EDX studies of the corrosion inhibition of copper in aerated NaCl solutions. J Appl Electrochem 36(2):215–226
74. Ebenso EE, Obot IB (2010) Inhibitive properties, thermodynamic characterization and quantum chemical studies of secnidazole on mild steel corrosion in acidic medium. Int J Electrochem Sci 5:2012–2035
75. El Azzouzi M, Aouniti A, Tighadouin S, Elmsellem H, Radi S, Hammouti B, El Assyry A, Bentiss F, Zarrouk A (2016) Some hydrazine derivatives as corrosion inhibitors for mild steel in 1.0 M HCl: weight loss, electrochemichal, SEM and theoretical studies. J Mol Liq 221:633–641
76. Tang L, Mu G, Liu G (2003) The effect of neutral red on the corrosion inhibition of cold rolled steel in 1.0 M hydrochloric acid. Corros Sci 45(10):2251–2261
77. Mu G, Li X, Li F (2004) Synergistic inhibition between o-phenanthroline and chloride ion on cold rolled steel corrosion in phosphoric acid. Mater Chem Phys 86(1):59–68
78. Elachouri M, Hajji MS, Salem M, Kertit S, Aride J, Coudert R, Essassi E (1996) Some nonionic surfactants as inhibitors of the corrosion of iron in acid chloride solutions. Corrosion 52(2):103–108
79. El Faydy M, Touir R, Touhami ME, Zarrouk A, Jama C, Lakhrissi B, Olasunkanmi LO, Ebenso EE, Bentiss F (2018) Corrosion inhibition performance of newly synthesized 5-alkoxymethyl-8-hydroxyquinoline derivatives for carbon steel in 1 M HCl solution: experimental, DFT and Monte Carlo simulation studies. Phys Chem Chem Phys 20:20167
80. Tayebi H, Bourazmi H, Himmi B, El Assyry A, Ramli Y, Zarrouk A, Geunbour A, Hammouti B (2014) Combined electrochemical and quantum chemical study of new quinoxaline derivative as corrosion inhibitor for carbon steel in acidic media. Der Pharm Chem 6(5):220–234
81. Tayebi H, Bourazmi H, Himmi B, El Assyry A, Ramli Y, Zarrouk A, Geunbour A, Hammouti B, Ebenso EE (2014) An electrochemical and theoretical evaluation of new quinoline derivative as a corrosion inhibitor for carbon steel in HCL solutions. Der Pharm Lett 6(6):20–34
82. Gomma GK, Wahdan MH (1995) Schiff bases as corrosion inhibitors for aluminium in hydrochloric acid solution. Mater Chem Phys 39(3):209–213
83. Durnie W, De Marco R, Kinsella B, Jefferson A (1999) Development of a structure–activity relationship for oil field corrosion inhibitors. J Electrochem Soc 146(5):1751–1756
84. Martinez S, Stern I (2002) Thermodynamic characterization of metal dissolution and inhibitor adsorption processes in the low carbon steel/mimosa tannin/sulfuric acid system. Appl Surf Sci 199(1–4):83–89
85. Abd El-Hameed RS (2011) Aminolysis of polyethylene terephthalate waste as corrosion inhibitor for carbon steel in HCl corrosive medium. Adv Appl Sci Res 2(3):483–499
86. El-Tabei AS, Hegazy MA (2013) A corrosion inhibition study of a novel synthesized gemini nonionic surfactant for carbon steel in 1 M HCl solution. J Surfact Deterg 16(5):757–766
87. Li DZ, Zhang SG, He B, Zhang LC (2009) Quantum chemistry study of the inhibitive properties of benzimidazoles. Comput Appl Chem 3:324–328
88. Gece G (2011) A review of promising novel corrosion inhibitors. Corros Sci 53(12):3873–3898
89. Daoud D, Douadi T, Issaadi S, Chafaa S (2014) Adsorption and corrosion inhibition of new synthesized thiophene Schiff base on mild steel X52 in HCl and H2SO4 solutions. Corros Sci 79:50–58
90. Hegazy MA, Badawi AM, Abd El Rehim SS, Kamel WM (2013) Corrosion inhibition of carbon steel using novel N-(2-(2-mercaptoacetoxy)ethyl)-N,N-dimethyl dodecan-1-aminium bromide during acid pickling. Corros Sci 69:110–122
91. Radilla J, Negron-Silva GE, Palomar-Pardave M, Romero-Romo M, Galvan M (2013) DFT study of the adsorption of the corrosion inhibitor 2-mercaptoimidazole onto Fe(1 0 0) surface. Electrochim Acta 112:577–586
92. Arslan T, Kandemirli F, Ebenso EE, Love I, Alemu H (2009) Quantum chemical studies on the corrosion inhibition of some sulphonamides on mild steel in acidic medium. Corros Sci 51(1):35–47
93. John S, Joseph A (2012) Electro analytical, surface morphological and theoretical studies on the corrosion inhibition behavior of different 1,2,4-triazole precursors on mild steel in 1 M hydrochloric acid. Mater Chem Phys 133(2–3):1083–1091